Research Square

Preprints are preliminary reports that have not undergone peer review.
They should not be considered conclusive, used to inform clinical practice,
or referenced by the media as validated information.

In-Situ Pin-Caulking: Effect of Self-Piercing Geometry and Pin Arrangement on Metal/CFRT Joints

Jan Gavelek

jan.gavelek@fau.de

Friedrich-Alexander-Universität Erlangen-Nürnberg

Leonie Elbel

Friedrich-Alexander-Universität Erlangen-Nürnberg

Marion Merklein

Friedrich-Alexander-Universität Erlangen-Nürnberg

Dietmar Drummer

Friedrich-Alexander-Universität Erlangen-Nürnberg

Research Article

Keywords: multi-material design, joining, in-situ caulking, self-piercing pin, continuous fibre-reinforced thermoplastic, joining force

Posted Date: November 5th, 2026

DOI: https://doi.org/10.21203/rs.3.rs-11456481/v1

License: This work is licensed under a Creative Commons Attribution 4.0 International License.
Read Full License

Additional Declarations: No competing interests reported.

Abstract

Multi-material design shifts the technological bottleneck from the components to the joining operation. In pin joining, metallic pin structures are formed and subsequently mechanically interlocked with a joining partner, enabling the joining of dissimilar materials without auxiliary elements. The in-situ pin caulking joining strategy combines hole formation, insertion and undercut generation in a single stroke, allowing the pin to act both as a forming element and as a load-carrying one, while the geometry after joining, rather than the extruded geometry, defines the interlock. A self-piercing pin (SP-Pin), whose thin walls are spread during the joining stroke, was compared with a solid cylindrical reference pin upset over its full cross-section. Both were joined to a unidirectional glass fibre/polypropylene laminate in four array configurations at constant pin spacing. Spreading the thin walls required less joining force than upsetting the full cross-section, without reducing the undercut. The normal load capacity of the SP-Pin was largely independent of the arrangement. That of the reference pin differed by a factor of 1.58 between the two-pin arrays. This indicates that the normal load capacity is governed mainly by the pin geometry for the SP-Pin and more strongly by the surrounding laminate for the reference pin. In the arrays, the SP-Pin largely maintained its shear force per unit joining force, unlike the reference pin. Despite a 25.0% lower joining force, the 2 × 2 SP-Pin joint carried 1.44 times the shear force and 2.87 times the normal force of the reference joint.

1 Introduction

Lightweight design increasingly relies on multi-material systems, in which continuous fibre reinforced thermoplastics (CFRT) are combined with metals so that each material is used where its specific properties are required. This shifts the technological bottleneck to the joining operation, since the pronounced differences in melting behaviour, thermal expansion and surface chemistry restrict the applicability of established techniques. Adhesive bonding provides a homogeneous stress distribution but requires demanding surface preparation and long curing times, and it fails abruptly once crack propagation has initiated [1]. Mechanical fastening by bolts or rivets, in contrast, necessitates a hole in the laminate, which severs load-bearing fibres and introduces stress concentrations that reduce the achievable bearing strength [2]. Against this background, penetrative reinforcement has emerged as a joining principle in which small metallic pins, extend from the metal part directly into the composite and thereby provide a geometrical interlock without an auxiliary element. The concept was first demonstrated for metal–composite laminates by Ucsnik et al. [3], who deposited pin structures onto the metal surface and embedded them during consolidation of the laminate. Parkes et al. [4] transferred the principle to additively manufactured pin arrays and showed that the pins delay failure initiation, slow down damage propagation and raise the ultimate strength of a single-lap joint by a factor of 6.5 relative to an unpinned reference, with an even more pronounced increase in absorbed energy. The scalability of such hybrid joining schemes towards structural component size was subsequently addressed in [5]. The mechanisms governing load transfer in pinned joints have been studied predominantly for pins that are geometrically invariant, i.e. that are inserted into the composite in their final shape. Chang et al. [6] identified the interaction of pin bending, matrix cracking and pin pull-out that determines the failure

sequence under monotonic and cyclic tension. Nguyen et al. [7] isolated the pull-out behaviour and demonstrated that the normal-direction capacity is limited by progressive pin extraction, and subsequently quantified the effect of pin geometry, support conditions and load introduction on the joint response [8]. A key finding across these studies is that the pin does not act as a rigid fastener but interacts with the surrounding fibre architecture: Eberl et al. [9] showed by full-field strain measurement that the fibre undulation formed around a pin dominates the local strain field and therefore the onset of failure. The competition between pin root fracture and pin extraction as limiting mechanisms, and its dependence on load severity, was recently characterised for static and fatigue loading in [10]. A consistent conclusion of this body of work is that a straight, cylindrical pin transfers normal loads almost exclusively by friction and residual clamping and is therefore prone to extraction. Löbel et al. [11] accordingly showed that a pin whose geometry provides a positive axial fixation, in their case staple-like elements, suppresses pull-out entirely and shifts failure into the composite. The manufacturing route of the pin determines which geometries are accessible. Additive manufacturing and electron beam surfi-sculpt, for which the relationship between process parameters and protrusion geometry was established in [12], offer high geometrical freedom at low deposition rates, while the insertion of separately manufactured pins introduces its own damage mechanisms in the laminate [13]. Cold forming is particularly attractive from a production point of view, since pins can be extruded directly out of the sheet plane in a short process chain and remain integral parts of the metal component. The corresponding forming limits, achievable pin heights and the local strain hardening of the pin were established in [14], and the extension towards non-rotationally symmetric pin geometries and their effect on joint quality was investigated in [15]. For thermoplastic matrix systems, cold formed pins can be embedded without pre-machining, because the matrix is locally melted and the fibres are displaced rather than severed. Popp et al. [16] analysed the resulting fibre deflection, matrix displacement and local consolidation and demonstrated that the characteristic fibre morphology around the pin, rather than the nominal contact area, determines the achievable strength. Building on this, undercutting pin geometries were introduced in combination with infrared heating in order to convert the frictional connection into an interlocking one and to counteract pin extraction [17]. An alternative route retains the interlock but generates it after insertion: in pin caulking the composite is perforated first, the pin is passed through the pre-formed hole and is subsequently upset into a head on the opposite side [18]. The present work employs in-situ pin caulking, in which hole formation and caulking are merged into a single stroke: the pin penetrates the locally heated composite and is upset within the same movement, so that the form-fit head is generated during, rather than after, the joining operation [19]. Because the pin is a forming element as well as a load-carrying one, its geometry is not preserved during joining, the pin shape after joining differs from the shape produced by extrusion, and it is the deformed geometry that defines the undercut and thus the normal-load capacity of the joint. This effect is particularly pronounced for self-piercing (SP) pin geometries, whose piercing cross-section is designed to be spread during the stroke. A comparable use is known from pin joining with pre-punched sheets, where the load-bearing capacity under axial loading is governed by the undercut formed through radial flaring of the pin head during joining rather than by the as-extruded pin geometry [20]. Therefore, the joining force is no longer a mere process quantity to be minimised, since part of it is expended on forming the interlock that carries the

load. Also unknown, the transition from the single pin to technically relevant multi-pin arrays, in which the pins interact both during the joining operation and under load. Sarantinos et al. [21] argued that a large number of small pins is preferable to a small number of large pins, since the damage introduced per pin scales with pin diameter while the interlocking area scales with pin number. This was confirmed experimentally in [22], where the pin density was kept constant while pin diameter and arrangement were varied. A higher number of smaller pins yielded superior performance under both shear and normal loading, which shows that joint strength does not scale linearly with pin number and that the mutual influence of adjacent pins must be accounted for.

The two central design decisions of an in-situ caulked pin joint, the pin type and the pin arrangement, have so far been investigated independently of one another .It is therefore unknown whether the deformation of an SP pin, and with it the interlock it generates, is affected when several pins are placed in close proximity and locally influence one another's material flow, and how the pin type affects the scaling of the joining force with the number of pins. The present study therefore compares a solid cylindrical pin and a self-piercing pin in four array configurations (1 × 1, 1 × 2, 2 × 1 and 2 × 2) at a constant pin spacing, joined by in-situ caulking. The joining force is recorded in-process and the mechanical performance is determined under shear and normal loading for every configuration, whereas the pin geometry before and after joining is compared by micrographs for the single-pin joint in order to quantify the interlock actually generated. Whether this interlock is maintained in the arrays is not documented directly, but is inferred from the arrangement dependence of the normal force, which is carried by the undercut. The objective is to separate the contribution of the pin type from that of the pin arrangement and to establish a quantitative relationship between the process force expended and the joint strength obtained.

2 Materials and Methods

2.1. Glass Fibre Composite

The continuously fibre reinforced thermoplastic (CFRT) sheets were manufactured by continuous compression moulding in an interval hot pressing process at NMF GmbH (Fürth, Germany). BJ100hp (Borealis AG, Vienna, Austria) was used as the matrix system. The reinforcing material was a non-crimp fabric consisting of unidirectionally (UD) oriented E-glass fibre rovings supplied by Saertex GmbH & Co. KG (Saerbeck, Germany) with an areal weight of 316 g/m². The manufactured laminate, comprising four reinforcing layers, had a thickness of approximately 1 mm and a fibre volume content of about 45%. After manufacturing, specimens measuring 105 mm × 45 mm for the shear tests and 150 mm × 50 mm for the cross-tension tests were cut from the sheets in accordance with DVS/EFB 3480-1 [23]. The fibre orientation of all specimens was aligned parallel to the long edge of the respective specimen. The laminate had a tensile strength of 541 ± 36 MPa in the fibre direction and 14.5 MPa perpendicular to the fibre direction, determined according to ISO 527-5 [24].

2.2. Steel Component

The metallic joining partner consists of the galvanised dual-phase steel HCT590X + Z (DP600). The material combines good formability with high mechanical strength and is therefore well suited for the forward extrusion of metallic pin structures and for industrial applications in the automotive sector [25]. A sheet thickness of 1.5 mm is selected to provide sufficient local material volume for multi-pin extrusion. The pins are manufactured using a multi-acting forming tool installed in a hydraulic press, type Lasco TSP 100, with a maximum forming force of 1000 kN. A schematic representation of the pin extrusion process and the relevant process parameters is shown in Fig. 1. Prior to forming, the steel sheet is lubricated on both sides with the extrusion oil Dionol ST V 1725-2 and positioned on the die. A blank holder subsequently fixes the sheet. The blank holder prevents lateral displacement and sheet buckling during forming while simultaneously controlling the material flow into the die cavities. Based on preliminary experience, a blank-holder stress of approximately 192 MPa is applied. Local material displacement into the die cavities is induced by individually configurable control punches. The control punches are actuated by a separate hydraulic power unit, allowing up to twelve pins to be extruded simultaneously by forward extrusion. The pin height is controlled by the punch penetration depth, which can be adjusted using a wedge adjustment mechanism. After forming, the steel sheet is removed from the die using ejector punches. Two different pin geometries are investigated. The reference pin is formed by conventional forward extrusion over its full cross-section, resulting in a solid cylindrical pin (see Fig. 1(b)). In contrast, fabrication of the self-piercing pins (SP-Pin) requires an additional preparation step prior to extrusion. At each pin position, a hole is drilled into the steel sheet before extrusion. This hole promotes a divided material flow during extrusion and results in the characteristic SP-Pin geometry, which resembles that of self-piercing riveting elements (see Fig. 1(a)). Based on preliminary investigations, a pre-hole diameter of 1.0 mm is selected. For all experiments, a mean pin height of 1.5 mm is extruded based on preliminary investigations. This height provides sufficient material for the formation of a pronounced undercut with a joining partner thickness of approximately 1.0 mm. Due to the reduced amount of material available for extrusion at the SP-Pin positions as a result of the pre-drilled holes, a greater punch penetration depth is required to obtain a comparable pin height.

2.3. Joining Process

All specimens were joined by the same in-situ process according to [19]. This process combines hole formation, joining and the creation of an undercut by pin caulking within a single process step. All multi-pin specimens were joined on a joining system (KLN Ultraschall AG, Heppenheim, Germany). Rather than adjusting the joining force individually for each specimen, the maximum system force of 16 kN was applied, thereby exceeding the required joining force in all configurations. The required joining force F_{req} was defined as the intersection of the tangent to the caulking stage (blue dotted line in Fig. 2) and the tangent to the compression of the entire structure (red dotted line in Fig. 2). Both tangents were obtained by linear regression over fixed intervals of the joining distance, from 0.6 mm to 0.8 mm for the caulking stage and from 0.9 mm to 1.0 mm for the compression of the entire structure. These intervals lie within the respective quasi-linear sections of the curve and were kept identical for all pin types and array configurations, so that F_{req} is defined consistently across the comparison. The construction was carried

out on each individual force-displacement curve, so that a mean value and a standard deviation could be assigned to the required joining force of every configuration. The laminate was heated by a medium-wave infrared emitter with a peak wavelength of approximately 2500 nm operated at a power setting of 100%. An aperture was used in every configuration to restrict the irradiation to the region intended to be softened and to shield the surrounding material. The aperture was adapted to each pin array such that the extent of the softened region, in which the fibres are mobile, corresponded per joining point to that of the single-pin reference: the entire area enclosed by the pins was heated, and the softened region extended beyond the outermost pins by the same margin in all configurations. This margin was adopted from Popp and Drummer [17], so that the minimum distance between the pin structure and the edge of the softened region was at least six times the pin diameter (6D) in every configuration. The thermal boundary conditions acting on an individual joining point were thereby kept comparable across all array sizes.

In the scope of this study, the two pin geometries introduced in the previous section – the SP-Pin and the solid cylindrical reference pin – were investigated on two specimen geometries in accordance with DVS/EFB bulletin 3480-1, with minor deviations. The lap shear specimen shown in Fig. 3 (a) featured an increased overlap of 28 mm in order to accommodate the multi-pin arrays. Due to the larger overlap, the total specimen length was reduced to 182 mm, whereas the free clamping length of 95 mm corresponded to the standard. The specimen width was 45 mm and the steel sheet thickness 1.5 mm. Normal loading was tested on the cross-tension specimen shown in Fig. 3 (b). Each sheet had outer dimensions of 150 mm × 50 mm, the central overlap resulting in a joined area of 50 mm × 50 mm. The cross-tension specimens were clamped via four holes of 20 mm diameter, each with an individual rectangular clamp. The pin arrays are designated m × n throughout this work, where m is the number of pin positions along the fibre direction of the laminate, which coincides with the long edge of the specimen and for the lap shear specimen, with the direction of the applied shear force and n the number of pin positions transverse to it, across the specimen width. A 2 × 1 array therefore comprises two pins placed one behind the other along the load and fibre direction, whereas a 1 × 2 array comprises two pins placed side by side across the width. The same designation applies to the cross-tension specimens, in which m refers to the fibre direction of the CFRT sheet. The pin array configurations are illustrated in Fig. 3 (c). The single pin (1 × 1) was located in the centre of the heated area at a distance of 14 mm from the ends of the overlap of the lap shear specimen. Both two-pin variants, 1 × 2 and 2 × 1, were investigated. The pin spacing was 12 mm, measured between the pin centres. Finally, the four-pin array (2 × 2) was investigated, in which the pins were arranged symmetrically about the centre with a spacing of 12 mm between the pin centres in both the horizontal and the vertical direction. The cross-tension specimens were configured in the same manner: the single pin was located in the centre, and the 1 × 2, 2 × 1 and 2 × 2 arrays were arranged symmetrically about the centre.

2.4. Microscopic Investigation

Cross-sections were prepared in order to document the change in pin geometry induced by the joining process and to characterise the resulting form-fit. For both pin types, sections were prepared after

joining in the 1 × 1 configuration, so that the initial and the deformed geometry could be compared directly and the undercut generated by pin caulking could be quantified. The single-pin joint was selected because it isolates the deformation of an individual pin from any influence between neighbouring joining points. The arrays were not sectioned; the interlock formed in them is instead assessed from the arrangement dependence of the mechanical response. The undercut u is defined as the radial overhang of the pin head over the pin shaft. Sections were prepared along the pin axis, parallel (0°) to the fibre direction of the outer layer. The specimens were embedded in epoxy resin with the application of vacuum. Owing to the surface tension of the resin, the cavity surrounding the pin was not always completely filled, which appears as black regions in the micrographs and was taken into account during evaluation. The sections were ground and polished and examined by reflected light microscopy using an Axio Imager.M2 equipped with an Axiocam 305 (Carl Zeiss Microscopy GmbH, Oberkochen, Germany).

2.5. Mechanical Characterisation

All specimens were tested to failure under standard climatic conditions of 23°C and 50% relative humidity in accordance with DIN EN ISO 291 [26]. Prior to testing, the specimens were stored under these conditions for at least 24 h to ensure complete conditioning. Three specimens were tested for each configuration (n = 3). A preload of 8 N was applied to the lap shear specimens and of 2 N to the cross-tension specimens, and a testing speed of 1 mm/min was used throughout. The displacement of the lap shear specimens was recorded by extensometers with a gauge length of 50 mm, which remained attached to the specimens until failure, whereas the displacement of the cross-tension specimens under normal loading was derived from the crosshead travel. All tests were carried out on a universal testing machine Zwick Z-1465 (ZwickRoell GmbH & Co. KG, Ulm, Germany). In addition to the maximum force, the stiffness of the joint was evaluated from the force - displacement curves. The stiffness was determined as the slope of a linear regression fitted between 10% and 40% of the maximum force of the respective specimen. Linearity within this range was verified by means of the coefficient of determination, a value of $R^2 \geq 0.97$ being required for all evaluated curves. Defining the evaluation range relative to the individual maximum force rather than as a fixed force or displacement interval ensured that the same section of the curve was evaluated for all configurations despite their differing load levels. As the displacement of the cross-tension specimens was derived from the crosshead travel, the corresponding stiffness values include the compliance of the testing set-up and are therefore only compared with one another, and not with the values obtained under shear loading.

3 Results and Discussion

3.1. Process properties and pin structure

Figure 4 (a) and (b) show the force–displacement curves recorded during joining for the SP-Pin and the reference pin. The minimum joining force is set to 100 N to reduce the data, therefore the joining distance showed below does not include Pin insertion into the CFRT. Figure 4 (c) summarises the required joining force derived from these curves.

For both pin types and all array sizes, the measured curves reproduce the process stages described above. The penetration of the pins into the laminate is completed at a joining distance of approximately 0.4 mm, up to which the force remains below 2 kN. The caulking of the pins takes place between approximately 0.4 mm and 0.9 mm and is characterised by an almost linear force increase. The subsequent steep rise corresponds to the compression of the entire structure. As the maximum system force was applied in every configuration, all curves terminate at a comparable level of approximately 16 kN. F_{req} was evaluated from each individual curve.

The SP-Pin requires a lower joining force than the reference pin in every configuration. The reduction amounts to 12.6% for the 1 × 1 joint (2.12 kN compared with 2.42 kN), 16.9% for the 1 × 2 array (3.97 kN compared with 4.78 kN) and 13.7% for the 2 × 1 array (4.24 kN compared with 4.91 kN). The largest difference occurs for the 2 × 2 array, where F_{req} decreases from 9.88 kN to 7.41 kN, which corresponds to 25.0%. Normalisation to the number of pins reveals that the two pin types respond differently to an increasing array size. For the reference pin, the force per pin remains within + 2.1% and − 1.3% of the single-pin value in all arrays and reaches 2.47 kN for the 2 × 2 array, so that F_{req} scales by a factor of 4.08 when the number of pins is quadrupled. For the SP-Pin, the force per pin decreases to 1.85 kN in the 2 × 2 array, corresponding to a scaling factor of 3.50. In the two-pin arrays the effect is not yet consistently resolved. The force per pin lies 6.1% below the single-pin value for the 1 × 2 array (1.99 kN) but is identical to it for the 2 × 1 array (2.12 kN), so that the sublinearity only becomes clear once all four joining points are present. Both observations are attributed to the different deformation mechanisms of the two pin types. The reference pin is upset over its full cross-section, so that the required force is governed by the flow stress acting on the entire cross-sectional area. This contribution is set by the pin material and is not affected by the presence of neighbouring joining points, which is consistent with the linear scaling observed. The wall segments of the SP-Pin are bent outwards instead. Since the bending moment of a thin wall segment scales with the square of the wall thickness, a considerably lower force is sufficient to form the undercut, and a correspondingly larger share of F_{req} is expended on the laminate itself: the self-piercing geometry splits the laminate locally and displaces the material into the pin cavity instead of pushing it aside. This laminate-related share depends on the local constraint and consolidation state of the surrounding material, so that neighbouring piercing points decompress one another and the force per pin decreases. The 2 × 1 arrangement requires the slightly higher joining force for both pin types, by 136 N (2.8%) for the reference pin and by 270 N (6.8%) for the SP-Pin. Neither difference is significant at n = 3, and no mechanistic interpretation is attached to it here; it is reported because the same ordering is obtained for both pin types.

Figure 5 shows cross-sections of the joined pin structures for the SP-Pin and the reference pin. Both pin types form the intended undercut geometry, with the pin head widening towards the upper laminate surface. The head widths measured at the upper surface are 1.937 mm for the SP-Pin and 1.922 mm for the reference pin. At the lower laminate surface the pin foot diameter amounts to 1.499 mm and 1.574 mm, so that the radial undercut is 0.22 mm for the SP-Pin and 0.17 mm for the reference pin. The undercut of the SP-Pin is not smaller than that of the reference pin, and it is generated at a joining force

that is 12.6% lower in the same configuration. The difference is consistent with the deformation mechanism proposed above and with the reduced joining force. The material is displaced into the pin interior rather than into the surrounding laminate, which supports the interpretation of the laminate-related share of the joining force and of the sublinear force scaling observed for the SP-Pin.

3.2. Mechanical Characterisation

Shear loading

Figure 6 summarises the maximum shear force, the energy absorbed up to F_{max} and the shear stiffness. The SP-Pin exceeds the reference pin in every configuration. The increase amounts to 35% for the 1 × 1 joint (203 N compared with 150 N), 32% for the 1 × 2 array (373 N compared with 283 N) and 28% for the 2 × 1 array (345 N compared with 270 N). As for the required joining force, the largest difference occurs for the 2 × 2 array, where the shear force increases by 44% from 505 N to 727 N. Normalisation to the number of pins reveals the expected loss of efficiency with increasing array size for both pin types, which is attributed to the non-uniform load distribution characteristic of multi-point mechanical joints, in which the outer joining points are engaged first and to a greater extent. The reference pin retains approximately 84% of its single-pin shear force per pin in the 2 × 2 array, whereas the SP-Pin retains approximately 90%. The total shear force therefore scales with a factor of 3.58 for the SP-Pin and 3.37 for the reference pin when the number of pins is quadrupled.

The comparison of the two two-pin arrays isolates the influence of the arrangement at constant pin number. The 1 × 2 array, in which the pins are placed side by side transverse to the shear force, reaches 373 N for the SP-Pin and 283 N for the reference pin, whereas the 2 × 1 array, in which the pins are aligned one behind the other parallel to the shear force and to the fibre direction, reaches 345 N and 270 N. The difference amounts to 28 N (8.1%) for the SP-Pin and to 13 N (4.8%) for the reference pin. For both pin types it is of the same order as the larger of the two standard deviations shown in Fig. 6(a). With three specimens per configuration a difference of this size cannot be separated from the scatter between specimens, and it is therefore not regarded as statistically confirmed. It is reported because the ordering is the same for both pin types. This ordering would be consistent with the fibre morphology that governs load transfer in pinned CFRT joints [16]. In the 1 × 2 arrangement each pin engages a separate group of fibre bundles across the specimen width, whereas in the 2 × 1 arrangement both pins lie on the same fibre bundles, so that the local reinforcement architecture is shared rather than duplicated. At the present sample size this explanation remains a hypothesis.

The energy absorbed up to F_{max} follows the same ranking, with the SP-Pin exceeding the reference pin by factors between 1.2 and 1.7. The absolute values increase disproportionately with array size, from approximately 0.05 J to 0.46 J for the SP-Pin, which indicates that the additional pins contribute not only load-bearing capacity but also displacement capability before the maximum force is reached.

The shear stiffness does not follow the number of pins. The configurations group in pairs according to the second index n, i.e. the number of pin positions transverse to the load: 1 × 1 and 2 × 1 (n = 1) reach

approximately 2700 N/mm and 2800 N/mm for the SP-Pin, whereas 1 × 2 and 2 × 2 (n = 3) reach approximately 3900 N/mm and 3830 N/mm. The reference pin shows the same ordering at a consistently lower level, though with larger scatter. Adding a second pin behind the first along the load path therefore does not increase the stiffness of the joint, while adding a pin next to it does. Pins arranged transverse to the load act as parallel load paths and widen the effectively joined cross-section. Pins arranged along the load path are engaged sequentially, and the compliance of the joining partners between them offsets the stiffness that is gained.

Normal loading

Under normal loading (Fig. 7) the difference between the two pin types is more pronounced than under shear loading. The SP-Pin carries 2.8 times the normal force of the reference pin in the 1 × 1 joint (83 N compared with 30 N), 1.9 times in the 1 × 2 array (127 N compared with 68 N), 3.2 times in the 2 × 1 array (139 N compared with 43 N) and 2.9 times in the 2 × 2 array (255 N compared with 89 N). The difference is even larger for the energy absorbed up to F_{max}, where the SP-Pin exceeds the reference pin by factors between 2.7 and 7.7. The relative scatter also differs systematically: the standard deviation of the SP-Pin amounts to between 3% and 13% of the mean value, whereas the reference pin reaches approximately 20% in several configurations.

For the SP-Pin, the normal force of the 1 × 2 and 2 × 1 arrays differs by only 8.6% (127 N compared with 139 N), whereas for the reference pin the same change of arrangement alters the normal force by a factor of 1.58 (68 N compared with 43 N), which is well outside the scatter of both configurations.

The 2 × 2 array of the reference pin follows the same pattern. Its normal force (89 N) corresponds to approximately twice that of the 2 × 1 array (43 N) rather than twice that of the 1 × 2 array (68 N). A mechanism that is set by the pin geometry alone is not expected to depend on the arrangement. The largely arrangement-independent normal force of the SP-Pin is consistent with such a mechanism. The arrangement dependence of the reference pin indicates that its normal load capacity is governed to a larger extent by the laminate surrounding the pin.

One possible explanation is that friction and residual clamping at the pin shaft carry a larger share of the normal load for the reference pin than for the SP-Pin. Both depend on the fibre morphology and the local consolidation state established around the pin during joining. In the 2 × 1 arrangement, both pins displace the same fibre bundles, as already assumed for shear loading. The fibre morphology and clamping at each joining point may therefore differ from those in the 1 × 2 arrangement. Splitting of the laminate parallel to the fibres could equally explain the arrangement dependence. Under axial load, the tapered reference pin loads the surrounding laminate radially. The tensile strength of the laminate perpendicular to the fibres is only 14.5 MPa. In the 2 × 1 arrangement, splits initiated at one pin would run towards the neighbouring pin. Both pin types form an undercut of comparable radial extent (Fig. 5). The normal force of the SP-Pin is nevertheless higher by factors between 1.9 and 3.2. The radial undercut alone does not account for this difference, since it is only 26% larger for the SP-Pin (0.22 mm compared with 0.17 mm). The two heads also differ in contour. The head of the SP-Pin is formed by the

spread wall segments. The reference head tapers continuously from the pin foot to the upper laminate surface. The contour may therefore contribute to the difference in addition to the overhang. A quantitative separation of overhang and contour would require a dedicated variation of the head geometry and is beyond the scope of the present comparison.

The normal stiffness increases monotonically with the number of pins, from approximately 66 N/mm for the single SP-Pin to 92 N/mm and 84 N/mm for the two-pin arrays and 151 N/mm for the 2 × 2 array. The increase is sublinear: doubling the number of pins raises the stiffness by a factor of 1.3 to 1.4, quadrupling it by a factor of 2.3. This is in part a consequence of the evaluation, since the displacement of the cross-tension specimens was derived from the crosshead travel and the compliance of the testing set-up is contained in every value, which compresses the differences between the configurations. Decisive for the present comparison is that the two two-pin arrays differ by only 8 N/mm, so that the normal stiffness is governed by the number of pins and not, as under shear, by their arrangement relative to the load. Under normal loading all pins act as parallel load paths irrespective of their position. The only configuration in which the reference pin reaches a nominally higher normal stiffness than the SP-Pin is the 1 × 2 array, at 98 N/mm compared with 92 N/mm. As Fig. 7(c) shows, the values of the two pin types lie close together in all configurations, although their normal forces differ by factors of 1.9 to 3.2. This is likewise attributed in part to the evaluation. The compliance of the testing set-up acts in series with that of the joint, so that the measured values are lower bounds of the joint stiffness and level out as the joint becomes stiffer. An exact determination of the normal stiffness therefore requires a displacement measurement directly at the joining point, either optically by digital image correlation or by a displacement transducer between the two sheets. Such a local measurement is foreseen for subsequent investigations.

Load direction and process efficiency

Considering both load directions together, the ratio of maximum shear force to maximum normal force characterises the anisotropy of the joint. For the reference pin this ratio lies between 4.2 and 6.3, whereas for the SP-Pin it lies between 2.5 and 2.9 and is almost independent of the configuration. The SP-Pin therefore not only increases the absolute load-bearing capacity but also produces a considerably more balanced joint, which is relevant for structural applications in which the loading direction is not known a priori or in which peel components are superimposed on the in-plane load. Relating the mechanical performance to the joining force combines the process and the performance perspective. For the SP-Pin the shear force per unit required joining force remains constant across the array configurations, at 96 N/kN for the 1 × 1 and 98 N/kN for the 2 × 2 joint, whereas for the reference pin it decreases from 62 N/kN to 51 N/kN, corresponding to a loss of 18%. Under normal loading both pin types lose efficiency. The SP-Pin decreases by 12% from 39.2 N/kN to 34.4 N/kN, the reference pin by 27% from 12.4 N/kN to 9.0 N/kN. The reason for this becomes clear when the scaling factors are compared directly. For the SP-Pin, F_{req} scales by a factor of 3.50 when the number of pins is quadrupled while the shear force scales by 3.58, so that process effort and load-bearing capacity increase at practically the same rate. For the reference pin, F_{req} scales by 4.08 while the shear force scales by only

3.37, so that the two trends diverge. The advantage of the SP-Pin therefore does not reduce as the array is enlarged. From a manufacturing point of view, this is the practically decisive result of the present study: the 2 × 2 SP-Pin joint provides 1.44 times the shear force and 2.87 times the normal force of the corresponding reference joint while requiring 25.0% less joining force.

4 Conclusion and Outlook

In-situ pin caulking merges hole formation, insertion and undercut generation into a single stroke, so that the pin is a forming element as well as a load-carrying one. A self-piercing pin and a solid cylindrical reference pin upset over its full cross-section were compared in four array configurations at constant pin spacing. The SP-Pin required a lower joining force in every configuration, from 12.6% for the single pin to 25.0% for the 2 × 2 array, while forming an undercut at least equivalent to that of the reference pin. This follows from the deformation mechanism: the reference pin is upset against the flow stress acting on its entire cross-section, whereas the wall segments of the SP-Pin are bent outwards, and the bending moment of a thin wall scales with the square of the wall thickness. It is therefore the geometry after joining, not the extruded geometry, that determines the interlock. The mechanical response supports this distinction. Under shear the SP-pin exceeded the reference pin by 28% to 44%, and the shear stiffness grouped according to the number of pin columns transverse to the load rather than the pin number.

Under normal loading the difference reached factors of 1.9 to 3.2. The normal force of the SP-Pin was largely insensitive to the arrangement (8.6% between the two two-pin arrays). That of the reference pin changed by a factor of 1.58. This indicates that the normal load capacity is governed mainly by the pin geometry for the SP-Pin and more strongly by the laminate around each joining point for the reference pin. Pin type and arrangement are accordingly coupled: the shear force per unit joining force remained constant for the SP-Pin across all array sizes but decreased by 18% for the reference pin, so that the 2 × 2 SP-Pin joint provided 1.44 times the shear force and 2.87 times the normal force of the reference joint at 25.0% less joining force.

The small share of the joining force expended on spreading the pin walls raises a question the present configuration does not answer. It is unclear whether the pin must penetrate the laminate at all. In the present setup the head is formed against the lower sample holder, which acts as the counter-die. If the reaction of the laminate itself were sufficient to spread the wall segments, the undercut could be generated within the laminate thickness and the pin would not emerge on the opposite side. Such an embedded variant would retain the form fit while leaving the distal surface closed, which is relevant for sealing, corrosion protection and visible-surface quality. It would also confine fibre severance to the penetrated depth and decouple the pin height from the laminate thickness. A further lever is the head contour itself. A geometry that spreads progressively and displaces the fibres around the expanding wall segments, rather than cutting them, would preserve the in-plane reinforcement adjacent to the joint.

Declarations

Funding statement

This work was funded by the German Research Foundation (DFG) within the scope of the transregional Collaborative Research Centre 285 on Method development for mechanical joinability in versatile process chains in the subproject C01 Joining without auxiliary elements Project- ID TRR 285/2–418701707. The authors thank the German Research Foundation for their organizational and financial support.

Author Contribution

All authors contributed to the study's conception and design. J.G. built the joining setup, including the joining tools. The metal components were manufactured by L.E. Preparation of the CFRT components, the joining experiments and data collection were performed by J.G. Analysis of the acquired data was performed by J.G. The original draft was written by J.G. M.M. and D.D. contributed to review and editing of the original draft as well as to supervision. All authors read and approved the final manuscript.

Acknowledgement

Funded by the Deutsche Forschungsgemeinschaft (DFG, German Research Foundation) – TRR 285/2 – Project-ID 418701707. The authors thank the German Research Foundation for their organisational and financial support.

Data Availability

Data will be made available on reasonable request.

References

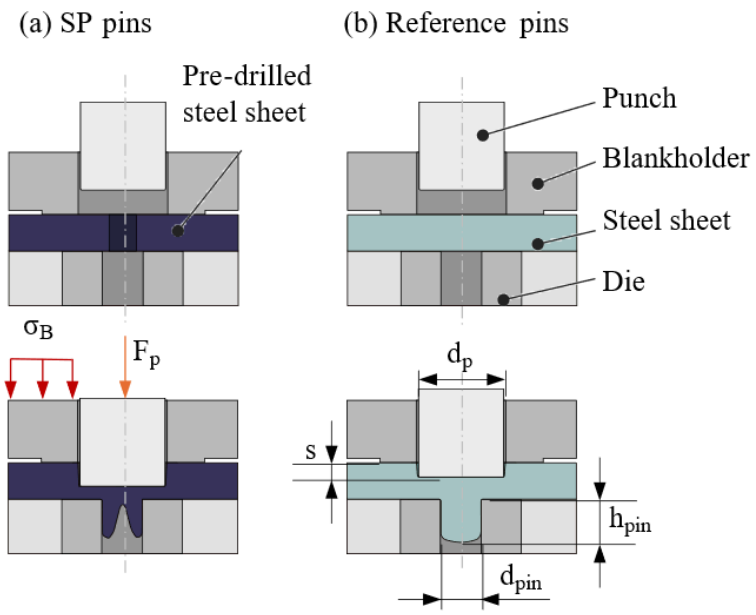
1. Galińska, A., Galiński, C.: Mechanical Joining of Fibre Reinforced Polymer Composites to Metals-A Review. Part II: Riveting, Clinching, Non-Adhesive Form-Locked Joints, Pin and Loop Joining. Polymers. **12**(8) (2020). 10.3390/polym12081681
2. Pramanik, A., Basak, A.K., Dong, Y., Sarker, P.K., Uddin, M.S., Littlefair, G., Dixit, A.R., Chattopadhyaya, S.: Joining of carbon fibre reinforced polymer (CFRP) composites and aluminium alloys – A review. Compos. Part A: Appl. Sci. Manufac. **101**, 1–29 (2017). 10.1016/j.compositesa.2017.06.007
3. Ucsnik, S., Scheerer, M., Zaremba, S., Pahr, D.H.: Experimental investigation of a novel hybrid metal–composite joining technology. Compos. Part A: Appl. Sci. Manufac. **41**(3), 369–374 (2010). 10.1016/j.compositesa.2009.11.003
4. Parkes, P.N., Butler, R., Meyer, J., de Oliveira, A.: Static strength of metal-composite joints with penetrative reinforcement. Compos. Struct. **118**, 250–256 (2014).

10.1016/j.compstruct.2014.07.019

5. Graham, D.P., Rezai, A., Baker, D., Smith, P.A., Watts, J.F.: The development and scalability of a high strength, damage tolerant, hybrid joining scheme for composite–metal structures. Compos. Part A: Appl. Sci. Manufac. **64**, 11–24 (2014). 10.1016/j.compositesa.2014.04.018
6. Chang, P., Mouritz, A.P., Cox, B.N.: Properties and failure mechanisms of pinned composite lap joints in monotonic and cyclic tension. Compos. Sci. Technol. **66**(13), 2163–2176 (2006). 10.1016/j.compscitech.2005.11.039
7. Nguyen, A.T., Brandt, M., Feih, S., Orifici, A.C.: Pin pull-out behaviour for hybrid metal-composite joints with integrated reinforcements. Compos. Struct. **155**, 160–172 (2016). 10.1016/j.compstruct.2016.07.047
8. Nguyen, A.T., Amarasinghe, C.K., Brandt, M., Feih, S., Orifici, A.C.: Loading, support and geometry effects for pin-reinforced hybrid metal-composite joints. Compos. Part A: Appl. Sci. Manufac. **98**, 192–206 (2017). 10.1016/j.compositesa.2017.03.019
9. Eberl, L., Avila Gray, L., Zaremba, S., Drechsler, K.: The effect of fiber undulation on the strain field for pinned composite/titanium joints under tension. Compos. Part A: Appl. Sci. Manufac. **103**, 148–160 (2017). 10.1016/j.compositesa.2017.09.015
10. Kralovec, C., Dengg, A., Schagerl, M., Schiller, A., Bisagni, C., Loebbecke, M., Haubrich, J., Hanelt, R.: Static strength and fatigue life of pinned hybrid titanium-composite single-lap-shear joints. Compos. Struct. **354**, 118765 (2025). 10.1016/j.compstruct.2024.118765
11. Löbel, T., Kolesnikov, B., Scheffler, S., Stahl, A., Hühne, C.: Enhanced tensile strength of composite joints by using staple-like pins: Working principles and experimental validation. Compos. Struct. **106**, 453–460 (2013). 10.1016/j.compstruct.2013.06.020
12. Wang, X., Ahn, J., Bai, Q., Lu, W., Lin, J.: Effect of forming parameters on electron beam Surfi-Sculpt protrusion for Ti–6Al–4V. Mater. Design. **76**, 202–206 (2015). 10.1016/j.matdes.2015.03.065
13. Neale, G., Skordos, A.: Insertion of large diameter through-thickness metallic pins in composites. Mater. Design. **216**, 110559 (2022). 10.1016/j.matdes.2022.110559
14. Kraus, M., Merklein, M.: Potential of Joining Dissimilar Materials by Cold Formed Pin-Structures. J. Mater. Process. Technol. **283**, 116697 (2020). 10.1016/j.jmatprotec.2020.116697
15. Römisch, D., Kraus, M., Merklein, M.: Investigation of the influence of formed, non-rotationally symmetrical pin geometries and their effect on the joint quality of steel and aluminium sheets by direct pin pressing. Proceedings of the Institution of Mechanical Engineers, Part L: Journal of Materials: Design and Applications 236(6), 1187–1202 (2022). 10.1177/14644207221081408
16. Popp, J., Kleffel, T., Römisch, D., Papke, T., Merklein, M., Drummer, D.: Fiber Orientation Mechanism of Continuous Fiber Reinforced Thermoplastics Hybrid Parts Joined with Metallic Pins. Appl. Compos. Mater. **28**(4), 951–972 (2021). 10.1007/s10443-021-09892-0
17. Popp, J., Drummer, D.: Joining of continuous fiber reinforced thermoplastic/steel hybrid parts via undercutting pin structures and infrared heating. J. Adv. Join. Processes. **5**, 100084 (2022). 10.1016/j.jajp.2021.100084

18. Römisch, D., Popp, J., Drummer, D., Merklein, M.: Joining of CFRT-steel hybrid parts via hole-forming and subsequent pin caulking. Prod. Eng. Res. Devel. **16**(2–3), 339–352 (2022). 10.1007/s11740-021-01093-9
19. Gavelek, J., Rösel, U., Drummer, D.: In-Situ Pin Caulking: A Novel Process Route for CFRT - Steel Hybrid Joints. J. Adv. Join. Processes. **100428** (2026). 10.1016/j.jajp.2026.100428
20. Römisch, D., Kraus, M., Merklein, M.: Tailored material flow in pin-extrusion of sheet metal under varying material and geometric conditions for enhanced joining technology applications. Int. J. Mater. Form. **18**(2) (2025). 10.1007/s12289-025-01897-5
21. Sarantinos, N., Kostopoulos, V., Di Vita, G., Campoli, G., Bricout, L.: Micro-pins: the next step in composite–composite and metal–composite joining. CEAS Space J. **11**(3), 351–358 (2019). 10.1007/s12567-019-00251-1
22. Popp, J., Gavelek, J., Römisch, D., Merklein, M., Drummer, D.: Influence of the pin diameter to spacing ratio in metal/composite joints joined via metallic pin structures. J. Adv. Join. Processes. **12**, 100326 (2025). 10.1016/j.jajp.2025.100326
23. DVS/EFB 3480-1: Merkblatt Prüfung von Verbindungseigenschaften (2021)
24. DIN EN ISO: 527-5:2022-05, Kunststoffe_- Bestimmung der Zugeigenschaften_- Teil_5: Prüfbedingungen für unidirektional faserverstärkte Kunststoffverbundwerkstoffe (ISO_527-5:2021); Deutsche Fassung EN_ISO_527-5:2021. DIN Media GmbH, Berlin
25. Kaźmierski, T., Krawczyk, J., Frocisz, Ł.: Characteristic of DP600 Steel Produced in Hot Rolling Process. Arch. Metall. Mater. 1641–1648 (2023). 10.24425/amm.2023.146234
26. DIN EN: ISO 291:2008-08, Kunststoffe_- Normalklimate für Konditionierung und Prüfung (ISO_291:2008); Deutsche Fassung EN_ISO_291:2008. DIN Media GmbH, Berlin

Figures



	Parameter description	*Value*
σ_B	Blank holder pressure	192 MPa
F_p	Punch force	
d_p	Punch diameter	3 mm
d_{pin}	Pin diameter	1.5 mm
h_{pin}	Pin height	1.5 mm
s	Punch penetration depth	> 0.77 mm

Figure 1

Schematic illustration of the pin extrusion for (a) self-piercing (SP) pins, (b) cylindrical, reference pins and (c) tabular overview of the main process parameters

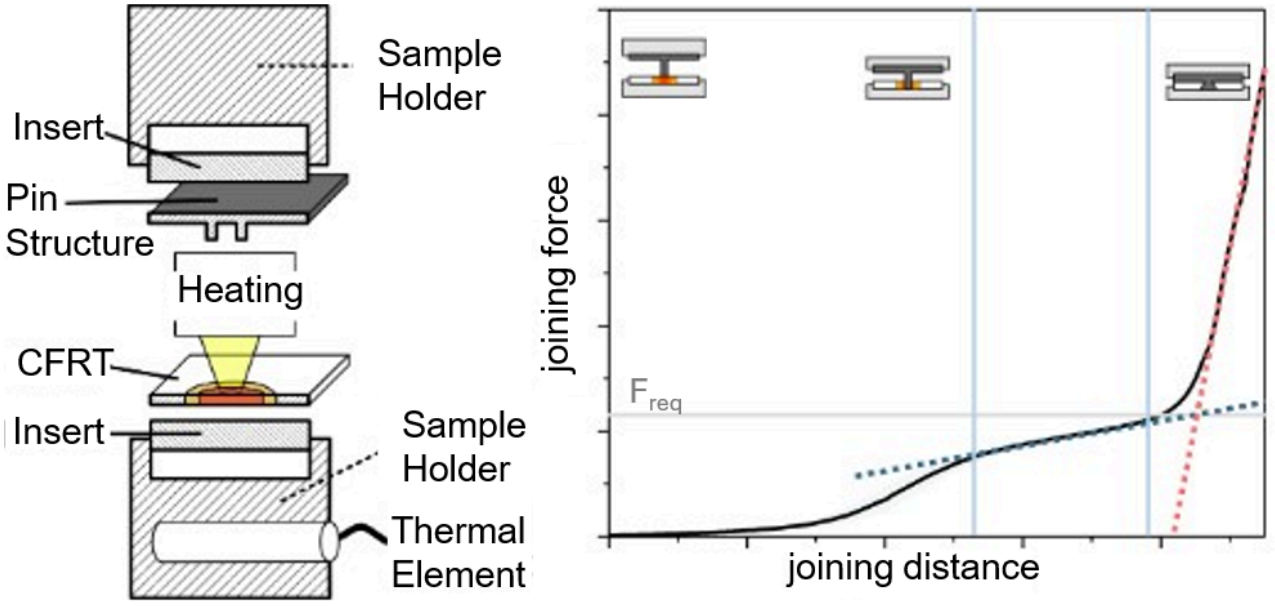


Figure 2

Assembly of the joining tool (left) with exemplary joining forces (right).

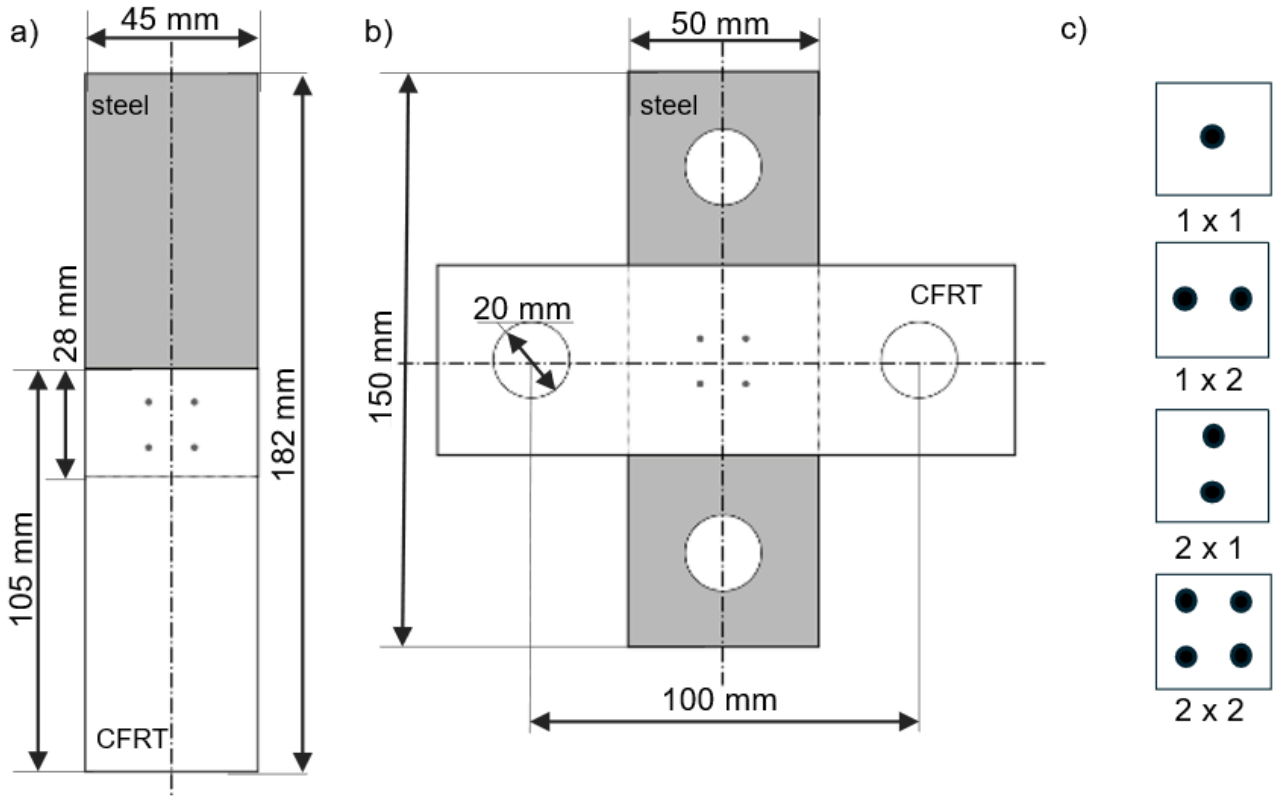


Figure 3

Specimen geometries used in this study: lap shear specimen (a), cross-tension specimen (b) and pin array configurations (c) for shear and normal load testing.

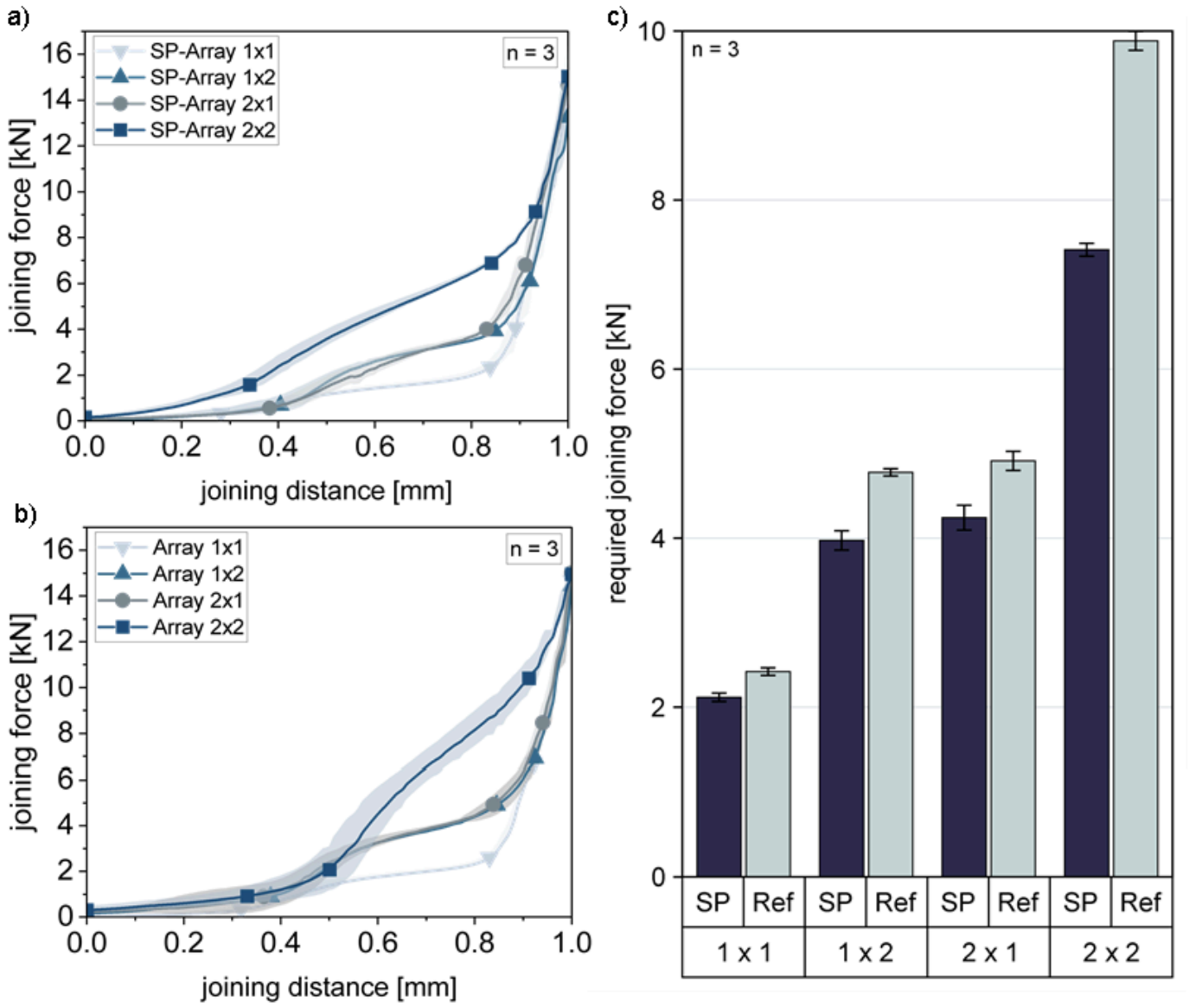


Figure 4

Joining forces for the self-piercing pins (a), reference pins (b) and the individual required joining force (c).

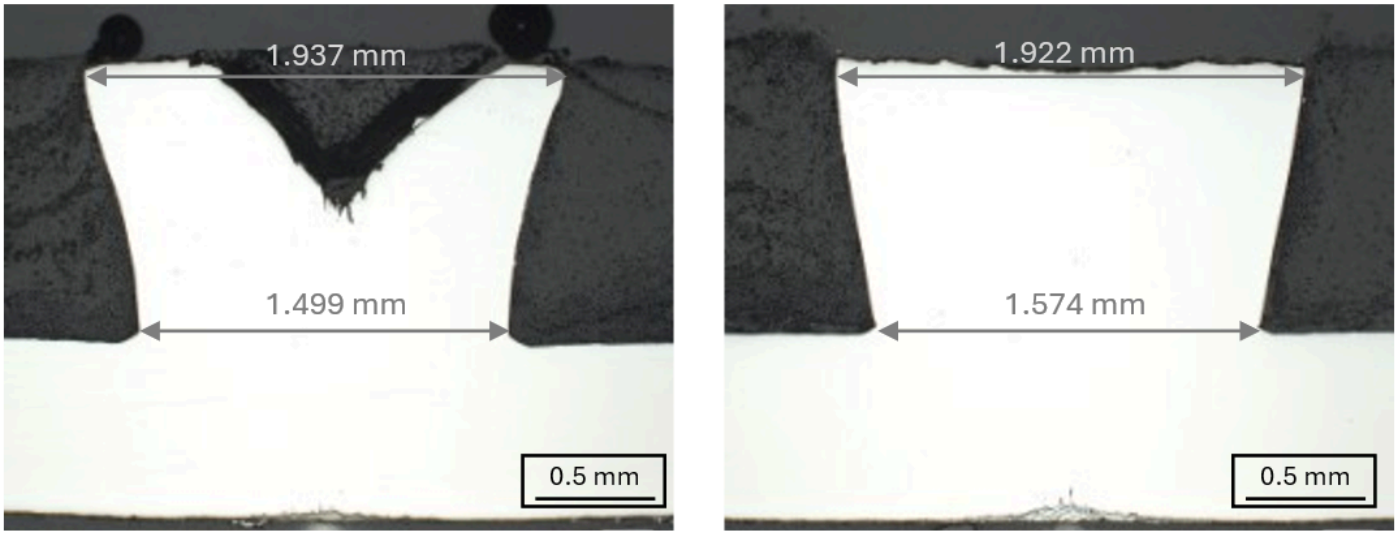


Figure 5

Cross-sections of the joined pin structures in the 1 × 1 configuration, (a) SP-Pin and (b) reference pin, showing the widths at the upper and lower laminate surface from which the radial undercut is obtained (0.22 mm for a, 0.17 mm for b).

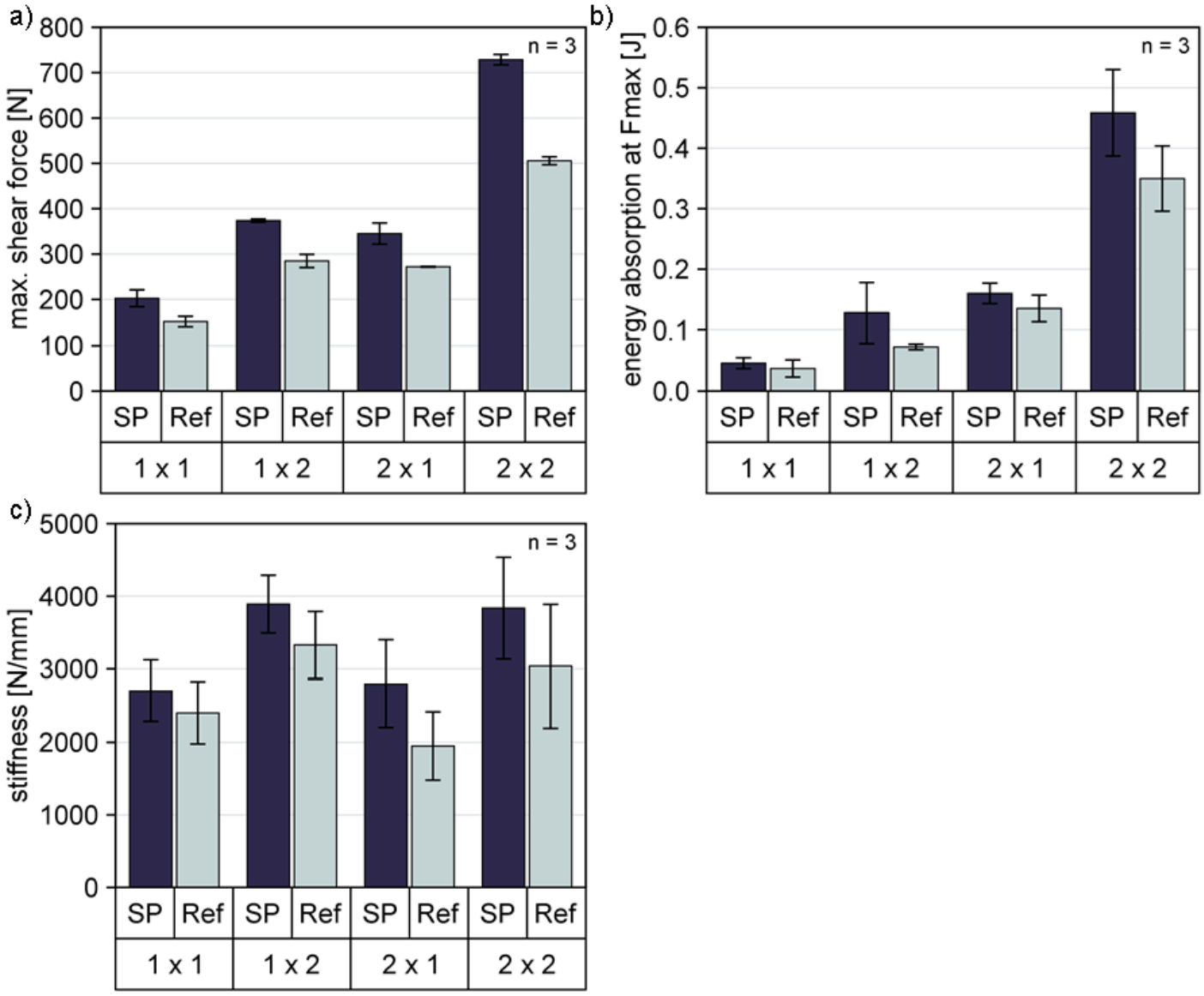


Figure 6

Shear test results for the SP-Pin and the reference pin in the four array configurations: maximum shear force (a), energy absorbed up to F_{max} (b) and shear stiffness (c).

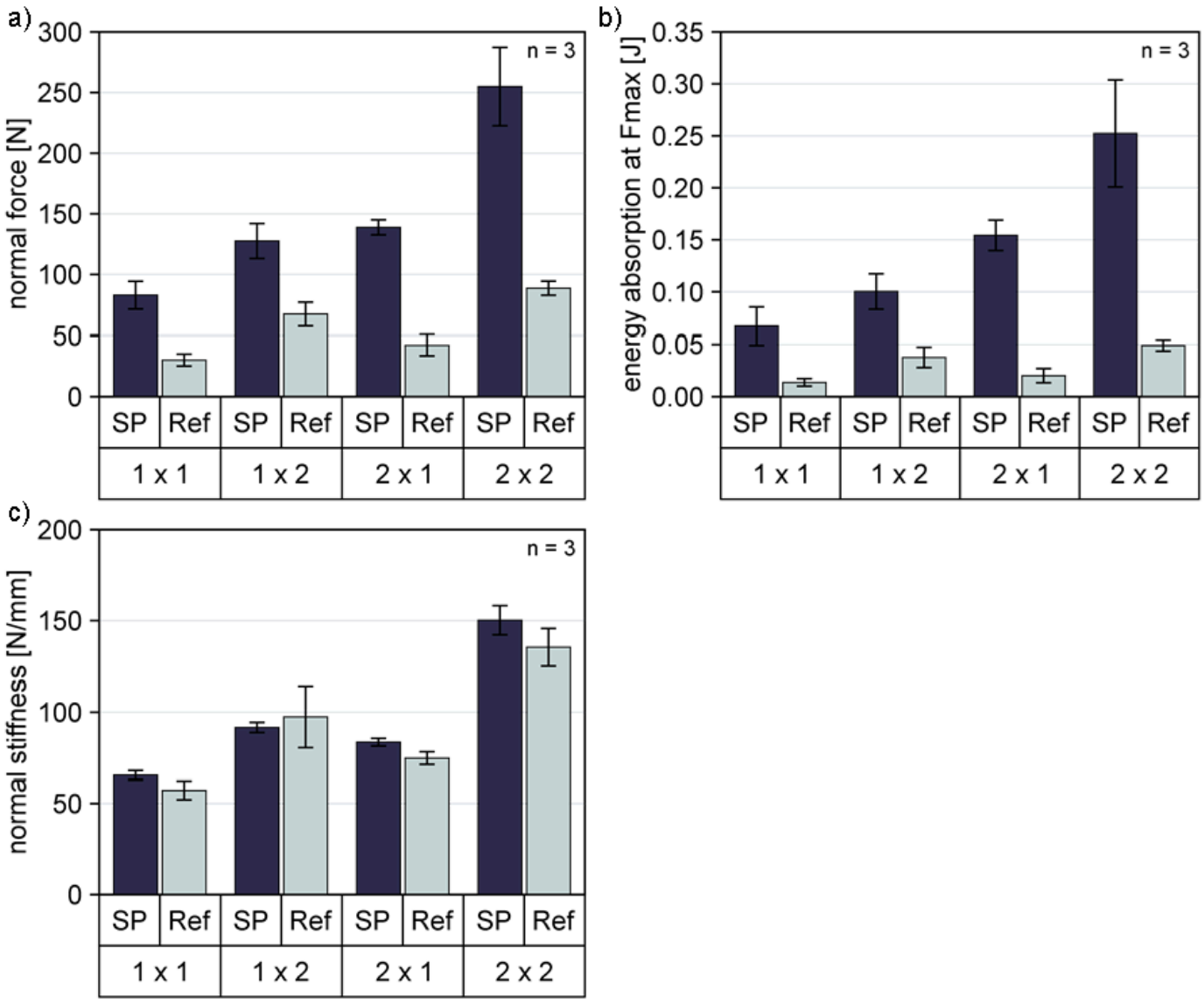


Figure 7

Cross-tension test results for the SP-Pin and the reference pin in the four array configurations: maximum normal force (a), energy absorbed up to F_{max} (b) and normal stiffness (c).